Mohd. Parvez Khan,[1] Abhishek Kumar Singh,[2] Amit Arvind Joharapurkar,[3] Manisha Yadav,[2] Sonal Shree,[4] Harish Kumar,[2] Anagha Gurjar,[2] Jay Sharan Mishra,[2] Mahesh Chandra Tiwari,[1] Geet Kumar Nagar,[1] Sudhir Kumar,[5] Ravishankar Ramachandran,[4] Anupam Sharan,[6] Mukul Rameshchandra Jain,[3] Arun Kumar Trivedi,[2] Rakesh Maurya,[5] Madan Madhav Godbole,[7] Jiaur Rahaman Gayen,[8] Sabyasachi Sanyal,[2] and Naibedya Chattopadhyay[1]

Pathophysiological Mechanism of Bone Loss in Type 2 Diabetes Involves Inverse Regulation of Osteoblast Function by PGC-1α and Skeletal Muscle Atrogenes: AdipoR1 as a Potential Target for Reversing Diabetes-Induced Osteopenia

Diabetes 2015;64:2609–2623 | DOI: 10.2337/db14-1611

Type 2 diabetes is associated with increased fracture risk and delayed facture healing; the underlying mechanism, however, remains poorly understood. We systematically investigated skeletal pathology in leptin receptor–deficient diabetic mice on a C57BLKS background (*db*). Compared with wild type (wt), *db* mice displayed reduced peak bone mass and age-related trabecular and cortical bone loss. Poor skeletal outcome in *db* mice contributed high-glucose– and nonesterified fatty acid–induced osteoblast apoptosis that was associated with peroxisome proliferator–activated receptor γ coactivator 1-α (PGC-1α) downregulation and upregulation of skeletal muscle atrogenes in osteoblasts. Osteoblast depletion of the atrogene muscle ring finger protein-1 (MuRF1) protected against gluco- and lipotoxicity-induced apoptosis. Osteoblast-specific PGC-1α upregulation by 6-C-β-d-glucopyranosyl-(2S,3S)-(+)-5,7,3′,4′-tetrahydroxydihydroflavonol (GTDF), an adiponectin receptor 1 (AdipoR1) agonist, as well as metformin in *db* mice that lacked AdipoR1 expression in muscle but not bone restored osteopenia to wt levels without improving diabetes. Both GTDF and metformin protected against gluco- and lipotoxicity-induced osteoblast apoptosis, and depletion of PGC-1α abolished this protection. Although AdipoR1 but not AdipoR2 depletion abolished protection by GTDF, metformin action was not blocked by AdipoR depletion. We conclude that PGC-1α upregulation in osteoblasts could reverse type 2 diabetes–associated deterioration in skeletal health.

Type 2 diabetes typically is a middle age–onset (>40 years) metabolic disease that affects multiple organ

[1]Division of Endocrinology, CSIR-Central Drug Research Institute, Lucknow, Uttar Pradesh, India
[2]Division of Biochemistry, CSIR-Central Drug Research Institute, Lucknow, Uttar Pradesh, India
[3]Zydus Research Centre, Ahmedabad, Gujarat, India
[4]Division of Molecular and Structural Biology, CSIR-Central Drug Research Institute, Lucknow, Uttar Pradesh, India
[5]Division of Medicinal and Process Chemistry, CSIR-Central Drug Research Institute, Lucknow, Uttar Pradesh, India
[6]Vinayak Cosmetic Surgery & Laser Centre, Lucknow, Uttar Pradesh, India
[7]Department of Endocrinology, Sanjay Gandhi Postgraduate Institute of Medical Sciences, Lucknow, Uttar Pradesh, India
[8]Division of Pharmacokinetics and Metabolism, CSIR-Central Drug Research Institute, Lucknow, UP, India

Corresponding author: Sabyasachi Sanyal, sanyal@cdri.res.in, or Naibedya Chattopadhyay, n_chattopadhyay@cdri.res.in.

Received 20 October 2014 and accepted 26 January 2015.

This article contains Supplementary Data online at http://diabetes.diabetesjournals.org/lookup/suppl/doi:10.2337/db14-1611/-/DC1.

M.P.K. and A.K.S. contributed equally to this work.

© 2015 by the American Diabetes Association. Readers may use this article as long as the work is properly cited, the use is educational and not for profit, and the work is not altered.

Downloaded from http://diabetesjournals.org/diabetes/article-pdf/64/7/2609/373668/db141611.pdf by guest on 14 May 2025

systems. Increasing evidence indicates that type 2 diabetes is associated with increased fracture risk, especially vertebral and hip fractures in older patients (1–4). Because chronic inflammation participates in diabetes pathogenesis and is a prerequisite for osteoclast activation, increased bone resorption is considered the likely cause of increased fracture risk in this disease. However, some studies intriguingly suggest that patients with type 2 diabetes have an increased risk of hip fractures at a higher bone mineral density (BMD) value than patients without diabetes (5) as well as an increased incidence of vertebral fractures at BMD values comparable to that of patients without diabetes (6). Thus, the reasons for increased skeletal fragility in patients with type 2 diabetes remain largely unexplained.

Patients with type 2 diabetes also have delayed fracture healing, resulting in poorer outcomes after hip fracture (7). Reduced fracture healing in type 2 diabetes is attributable to decreased collagen content, defective cross-linking, alterations in collagen subtype ratios, and collagen defects due to accumulation of advanced glycation end products (8–10), which could impair osteoblast function. These could also lead to compromised bone material strength and increased cortical porosity, affecting bone quality as shown in postmenopausal women with type 2 diabetes (11,12).

Several mouse models of type 2 diabetes are available; however, they poorly represent the human skeletal fragility observed in patients with typical type 2 diabetes (13). Unlike typical middle-aged type 2 diabetes onset in humans, when skeletal maturity has already been attained in genetically engineered diabetic mice, the onset of diabetes occurs at 4–8 weeks, an age comparable to adolescence in humans at which skeletal maturity has not been attained (14). However, the average onset age is falling in humans and is becoming increasingly common among those aged <30 years, including children and adolescents in various ethnic groups (15–18). This early-onset diabetes is characterized by increased disease severity and pancreatic β-cell failure than is typical of type 2 diabetes (19–21). Data on the impact of early-onset type 2 diabetes on human skeletal health are limited, although one report indicated that children with prediabetes with impaired glucose tolerance have low mineral content and low bone mass (22). We thus believe that the distinction in skeletal phenotype between early- and middle age–onset type 2 diabetes might be important for the following reason: Although skeletons of children/adolescents predominantly undergo modeling-directed growth (resulting in a net increase in bone mass due to enhanced osteoblastic activity), adult skeletons predominantly experience remodeling (no net bone gain), and thus, type 2 diabetes in these two cases may affect skeletal health differently.

Although monogenic obese and diabetic mouse models, such as leptin receptor–deficient diabetic mice, essentially differ from the polygenic disease origin in human type 2 diabetes, these may serve as a suitable model for deciphering the skeletal outcomes in this disease. We investigated the skeletal phenotype in leptin receptor–deficient genetically obese diabetic mice (in C57BLKS background) (*db*) that manifest severe diabetes, including pancreatic β-cell failure. The study also involved the identification of factors crucial for type 2 diabetes–induced skeletal effects. Furthermore, modulation of such factors by therapeutic intervention on diabetic skeleton was assessed.

RESEARCH DESIGN AND METHODS

Reagents and Kits

Cell culture reagents were from Life Technologies. Fine reagents were from Sigma-Aldrich unless indicated otherwise. Globular adiponectin (gAd) was from ATGen Global. ^{125}I (20 MBq) was from Bhabha Atomic Research Center (Mumbai, India). Kits for plasma biochemical parameters were glucose (Pointe Scientific), lipids and creatinine (Randox Laboratories Ltd., Mumbai, India), insulin (Millipore), adiponectin (B-Bridge International Inc.), and osteocalcin (OCN) (Uscn Life Science Inc.). ELISA kits were plasminogen activator inhibitor 1, MCP-1, leptin, and resistin (Millipore). The TUNEL assay kit was from Roche Applied Science. 6-C-β-d-glucopyranosyl-(2*S*,3*S*)-(+)-5,7,3′,4′-tetrahydroxydihydroflavonol (GTDF) (purity >98%) was purified as previously reported (23), and metformin (Met) (purity 97%) and pioglitazone (Pio) (purity ≥98%) were from Sigma-Aldrich.

Animal Experiments

Wild type (wt) (C57BLKS/J) or *db* (BKS.Cg-Dock7^{m} +/+ Lepr^{db}/J and B6.db; B6.BKS(D)-Lepr^{db}/J) mice were housed at 22 ± 3°C on a 12-h light/dark cycle. All animals had access to a standard chow diet and water ad libitum. Time course studies were conducted at the American Association for Laboratory Animal Care–accredited facility of Zydus Research Centre (ZRC) (Ahmedabad, India) following approval from the Institutional Animal Ethics Committee of ZRC. The *db* or wt mice used were originally from The Jackson Laboratory, and the colonies were maintained at ZRC. Drug treatment studies using 10-week-old *db* mice from Harlan Laboratories (the Netherlands) (BKS.Cg- + Lepr^{db}/+Lepr^{db}/OlaHsd) were conducted at Syngene International Ltd. (Bangalore, India) in its American Association for Laboratory Animal Care–accredited facility following ethical approval from the Institutional Animal Ethics Committee. In both studies, all the animals were randomized into groups based on blood glucose levels and body weight. Vehicle groups received 0.5% carboxymethylcellulose, and treatment groups received GTDF (10 mg/kg), Met (350 mg/kg), and Pio (10 mg/kg) once a day by oral gavage for 30 days. Doses of Met in adult humans range from 850 to 2,550 mg/day, which comes to 14.6–42.5 mg/kg (considering the average human weight to be 60 kg). The adult human dose of Pio is 15–45 mg/day, which corresponds to 0.25–0.75 mg/kg. The equation for dose translation from human to mouse

Downloaded from http://diabetesjournals.org/diabetes/article-pdf/64/7/2609/579698/db141611.pdf by guest on 14 May 2025

was based on body surface area: human equivalent dose (mg/kg) = animal dose (mg/kg) × (animal K_m/human K_m) (24). Feed intake and body weight were measured every day, and on day 31, the animals were killed. Plasma and tissues were collected and stored at −80°C until further analysis.

Microcomputed Tomography

Microcomputed tomography (μCT) of excised bones was carried out using a SkyScan 1076 CT scanner (Aartselaar, Belgium) as described earlier for mouse bone (25,26) and following the general guidelines for the assessment of bone microarchitecture in rodents using μCT (27). For scanning, source voltage was set to 50 kV and current to 200 μA. The X-ray source rotation step size was 0.84° over a trajectory of 180°. Reconstructions were made using NRecon version 1.6.9.4 software (SkyScan) to create two-dimensional (2D) 2,000 × 2,000–pixel images with a beam hardening correction set to 10% with dynamic range of −1,000 to 11,000 Hounsfield units. By drawing ellipsoid contours, trabecular bone was extracted using the CT analyzer software. In the femur epiphysis region, 200 slices were selected, leaving 50 slices from the start of the growth plate as a reference point. Cortical parameters were determined at femur mid-diaphysis by 2D analysis. From the start of the growth plate as a reference point, 200 slices were selected in the cortical region, leaving 500 slices as offset (to exclude the trabecular region). For BMD calibration, 2-mm-diameter hydroxyapatite phantom rods with known BMD (0.25 and 0.75 g/cm^3) were used. For each analysis, the estimated BMD was determined based on linear correlation between the μCT attenuation coefficient and BMD (28).

Bone Biomechanical Strength

Three-point bending test on femur was performed using a bone strength tester (TK-252C; Muromachi) as previously reported (29).

Determination of the Bone Lining Cells

Deparaffinized and hydrated femoral epiphysis sections (5 μm) of various groups were stained with hematoxylin-eosin (H-E), and bone lining cells were visualized by light microscopy. Ten sections per mouse (n = 6) were used for counting by two independent researchers blinded to the experimental design.

Cell Culture and Induction of Differentiation

Mouse calvarial osteoblasts (MCOs) were obtained from 1–2-day-old mouse pups as described earlier (26,30). Bone marrow cells from 10–12-week-old male wt and *db* mice were isolated, cultured, and differentiated into osteoblasts as described earlier (31).

Radioiodination of gAd and Radioligand-Binding Experiment

Ten micrograms gAd was radioiodinated by iodogen method using precoated iodination tubes (Pierce) according to the manufacturer's instructions. Excess ^{125}I was removed by a PD-10 desalting column (GE Healthcare). For binding assays, osteoblasts and myocytes in 24-well plates were incubated with increasing concentrations of ^{125}I-gAd in PBS supplemented with 0.1% BSA for 2 h (at which time binding equilibrium was achieved), after which the cells were washed and lysed. Nonspecific binding for each concentration was determined using a 200-fold excess of cold gAd. Specific binding was calculated by subtracting nonspecific binding from total binding.

RNA Interference Experiments

Small interfering (si) RNAs were from Dharmacon. MCOs were transfected with 0.1 μmol/L of each siRNA per well using DharmaFECT 1 transfection reagent (Dharmacon) in six-well plates. Seventy-two hours after transfection, cells were treated as indicated and analyzed as required.

Quantitative PCR, Immunoblotting, and Immunohistochemistry

These studies were performed using standard procedures as previously described (32,33). Primer sequences for quantitative PCR (qPCR) are listed in Supplementary Table 3. Antibodies and dilutions for immunoblotting were as follows: anti-peroxisome proliferator–activated receptor γ (PPARγ) coactivator 1-α (PGC-1α) (ST1202; Calbiochem; 1:2,000); anti-AMPK, phospho-AMPK (pAMPK) (Thr 172), and cleaved caspase-3 (Cell Signaling Technology; 1:1,000); and adiponectin receptor (AdipoR) 1, AdipoR2, muscle ring finger protein-1 (MuRF1), and β-actin antibodies (Santa Cruz Biotechnology; 1:1,000 except for β-actin, which was 1:3,000). TUNEL assay was performed as described earlier (33). For immunohistochemistry, femur epiphysis transverse sections (5 μm) were deparaffinized, hydrated, and after antigen retrieval, incubated with mouse anti-Runx2 (Abcam; 1:1,600) along with anti-PGC-1α (1:2,000), pAMPK (1:500), or MuRF1 (1:500) at 4°C overnight. The sections were then washed and incubated with fluorescent Alexa Fluor goat anti-mouse and goat anti-rabbit IgG (H + L) (1:1,500) (Life Technologies) for 1 h at room temperature. Sections were also stained with DAPI and visualized by fluorescent microscopy. Image-Pro Plus 6.1 software (Media Cybernetics) was used for quantification of microscopic data where five randomly selected fields from six bone sections per group were analyzed.

Osteoblast Differentiation Assay

MCOs at 70–80% confluence were trypsinized, and 2 × 10^3 cells/well were seeded in 96-well plates. After 24 h, cells were given various treatments for 48 h in osteoblast differentiation medium. Alkaline phosphatase (ALP) activity was measured using a fluorometric kit (BioVision) according to the manufacturer's protocol.

Cell Viability Assay

MCOs in 96-well plates (2 × 10^3 cells/well) were treated with increasing concentrations of glucose, palmitic acid, and dexamethasone (Dex) with or without GTDF and Met for 48 h. Osteoblast viability was assessed by

Downloaded from http://diabetesjournals.org/diabetes/article-pdf/64/7/2609/579698/db141611.pdf by guest on 14 May 2025

3-(4,5-dimethylthiazol-2-yl)-2,5-diphenyltetrazolium bromide (MTT) assay as previously reported (33).

Flow Cytometry–Based Determination of Apoptosis

Annexin V-FITC Apoptosis Detection kit (Sigma) was used to determine apoptosis. Briefly, the treated cells were trypsinized and washed with PBS, and 1×10^6 cells/mL were resuspended in binding buffer and labeled with 5 μL annexin V-FITC and 10 μL propidium iodide (PI) for 10 min in the dark. Cell fluorescence was measured on a FACSCalibur flow cytometer (Becton Dickinson) and analyzed using CellQuest Pro software.

Data Analysis and Statistics

Results are expressed as mean ± SE. All data were analyzed using GraphPad Prism 5.0 software. Statistical analyses were performed using one- or two-way ANOVA as appropriate followed by Bonferroni posttest analysis.

RESULTS

Lack of Peak Bone Mass Achievement and Age-Related Osteopenia in BKS.Cg-*Dock7^m* +/+ *Lepr^{db}*/J Mice

Three-dimensional μCT evaluation of trabecular microarchitecture in 8-, 12-, and 16-week-old C57BLKS/J (wt) and *db* mice revealed that *db* femur epiphysis at all ages displayed a loosely connected trabecular network compared with wt mice (Fig. 1*A*). The wt mice displayed bone gain at 12 weeks characterized by significantly higher BMD, trabecular bone volume (BV/TV), trabecular number (Tb.N), and connectivity density (Conn.D), followed by trabecular loss at 16 weeks manifested by decreases in these parameters (Fig. 1*A*). The *db* mice did not gain bone at any age and were osteopenic throughout, characterized by significantly lower BMD, BV/TV, Tb.N, trabecular thickness (Tb.Th), and Conn.D and higher trabecular separation (Tb.Sp) than wt mice (Fig. 1*A*). Age-based comparison in *db* mice also revealed progressive osteopenia characterized by significantly higher Tb.Sp at 16 weeks, and other parameters compared with 8-week-old *db* mice showed a decreasing trend with age.

Femur mid-diaphysis of *db* mice representing cortical bone showed a thinner cortex than wt mice at all ages (Fig. 1*B*). At 8 weeks, BMD, average cortical thickness (Ct.Th), and cortical area (Ct.Ar) were comparable between wt and *db*, the latter group displaying significantly lower periosteal perimeter (Ps.Pm) and endocortical perimeter (Ec.Pm). At 12 and 16 weeks, all cortical parameters in *db* were significantly lower than corresponding wt groups (Fig. 1*B*). Like trabecular parameters, cortical parameters, including BMD, Ct.Th, and Ct.Ar, in 12-week-old wt mice were significantly higher than 8-week-old wt mice, and at 16 weeks, these parameters displayed a decreasing trend compared with 8-week-old wt mice (Fig. 1*B*). The *db* mice showed no cortical gain at any age (Fig. 1*B*).

Osteoblast apoptosis is associated with both primary and secondary osteoporosis (34) and compared with wt femur epiphysis in *db* mice across all age-groups, displayed remarkably increased osteoblast apoptosis (Fig. 1*C* and Supplementary Fig. 1*A*). Periosteal or bone lining cells are a source of osteogenic precursors (35). At 12 weeks, wt but not *db* bones displayed significantly higher periosteal cell numbers than the 8-week groups (Fig. 1*D* and Supplementary Fig. 1*B*), and *db* mice at all ages had significantly lower periosteal cell numbers than wt mice (Fig. 1*D*). The osteogenic surrogate serum OCN level dropped significantly with age in both mice; however, as reported earlier (36), *db* mice had significantly lower OCN levels than wt mice (Fig. 1*J*).

Compared with wt, nonfasting and fasting glucose was significantly higher in 8-week-old *db* mice (>280 and >150 mg/dL, respectively), which further increased to >450 and >200 mg/dL at 12 weeks and remained steady thereafter (Fig. 1*E* and *F*). The *db* mice also displayed significant nonfasting and fasting hyperinsulinemia (Fig. 1*H* and *I*); however, insulin levels in 16-week-old *db* mice was significantly less than in 8-week-old *db* mice, probably due to β-cell apoptosis, which is typical of the *db* strain. Despite the decrease in insulin, 16-week-old *db* mice had intriguingly comparable blood glucose levels to that of 12-week-old *db* mice, although we cannot explain it. Presumably, this finding was due to elimination of glucose through urine, which again, is a trait in *db* mice. Nonesterified fatty acid (NEFA) level in *db* mice was significantly higher than wt at all ages, and no age-dependent change was observed (Fig. 1*G*). Consistent with earlier reports (37,38), *db* mice at 8 weeks displayed a significantly lower adiponectin level than wt, which decreased further with age (Fig. 1*K*).

Glucose and Palmitate Directly Induce Osteoblast Apoptosis

We next assessed whether NEFA and glucose, the two major mediators of diabetic pathology, could directly affect osteoblast viability. Both palmitate and glucose induced loss of MCO viability and apoptosis in vitro (Fig. 2*A* and *B*). Apoptosis-related cysteine protease caspase-3 activation assay revealed that palmitate and Dex but not glucose enhanced cleaved (active) caspase-3 levels (Fig. 2*C*).

db Mice Display Suppression of PGC-1α and Increase in Skeletal Muscle Atrogene Expression in Bone

Consistent with enhanced osteoblast apoptosis, *db* femur epiphysis displayed significantly higher p53 expression than wt at all ages (Fig. 3*A*). Among the *db* group, 16-week-old mice had significantly higher p53 than 8-week-old mice (Fig. 3*A*). Consistent with peak bone gain (Fig. 1*A* and *B*), wt mice displayed significantly higher Runx2 (key osteogenic factor) expression at 12 weeks followed by a decline at 16 weeks, whereas Runx2 mRNA in *db* femur epiphysis was significantly lower than wt at all ages (Fig. 3*A*). Furthermore, among the

Downloaded from http://diabetesjournals.org/diabetes/article-pdf/64/7/2609/579698/db141611.pdf by guest on 14 May 2025

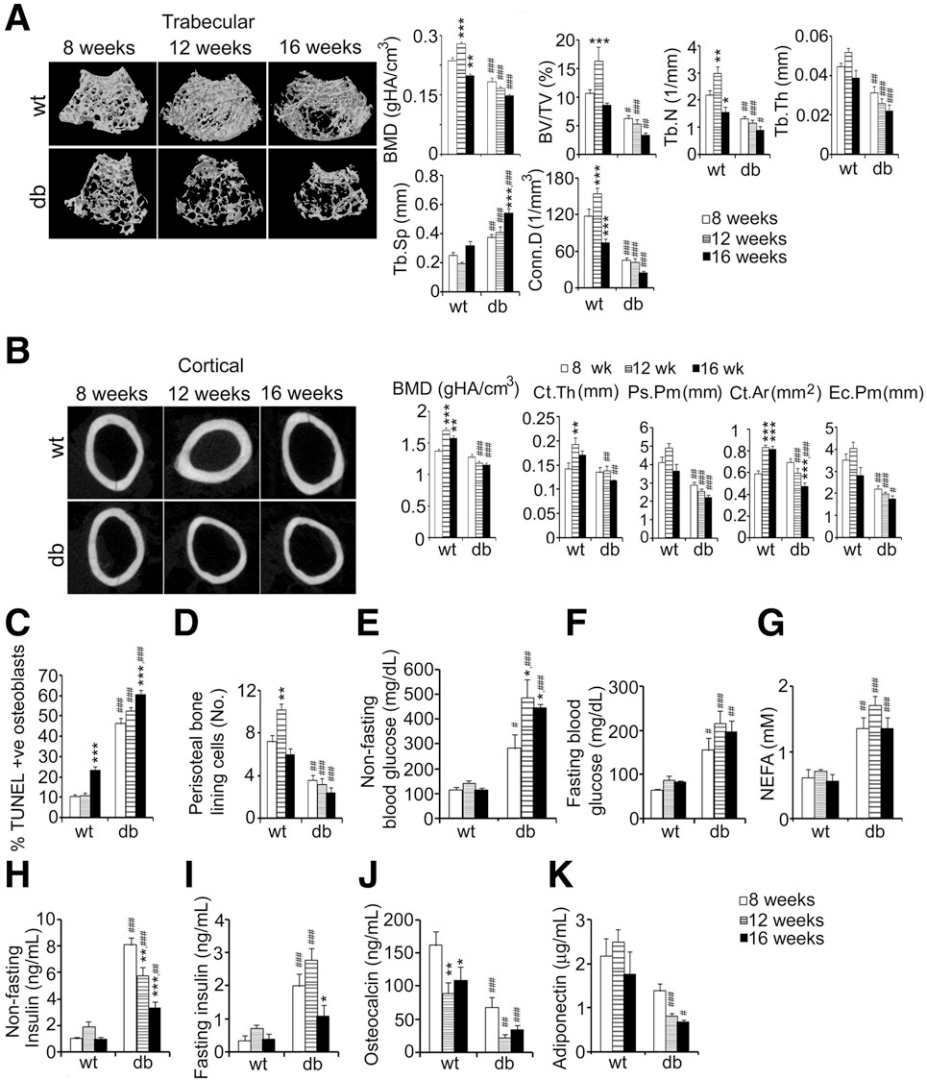

Figure 1—Evaluation of bone phenotypes in 8-, 12-, and 16-week-old wt and *db* mice. *A*: Age- and genotype-dependent changes in trabecular microarchitecture. A μCT analysis was carried out using a SkyScan 1076 CT scanner (Aartselaar, Belgium). The left panel shows representative images from three-dimensional μCT analysis of femur epiphyses (trabecular bone) from 8-, 12-, and 16-week-old wt and *db* mice. The bar graphs on the right show quantification. *B*: Age- and genotype-dependent changes in cortical parameters. Femur mid-diaphysis representing cortical bone was analyzed by μCT. The left panel shows 2D μCT representative images; the right panels show quantification. *A* and *B*: n = 6 bones/group. *C*: The *db* mice displayed enhanced osteoblast apoptosis. Quantification of apoptotic osteoblasts was performed by dual TUNEL (DNA fragmentation marker) and Runx2 (osteoblast marker) staining of femur epiphysis sections (6 bones/group, 5 fields/bone) followed by confocal microscopy (Carl Zeiss LSM 510 Meta, Jena, Germany). Runx2-positive and TUNEL-positive cells were plotted as a percent of total Runx2-positive cells (representative images shown in Supplementary Fig. 1*A*). *D*: The *db* mice displayed reduced bone lining cells. H-E–stained femur epiphysis sections (6 bones/group, 5 fields/bone) were used for counting by light microscopy by two independent researchers blinded to the experimental design (representative microscopic images shown in Supplementary Fig. 1*B*). *E–K*: Serum biochemical parameters in wt and *db* mice (n = 6/group). Data are mean ± SE. *Eight-week vs. 12- or 16-week age-groups. #wt vs. *db* (corresponding age-groups). *,#$P < 0.05$; **,##$P < 0.01$; ***,###$P < 0.001$ as determined by two-way ANOVA followed by Bonferroni posttest analysis. +ve, positive; Conn.D, trabecular connectivity normalized by tissue volume.

db group, Runx2 expression significantly declined with age (Fig. 3*A*).

Muscular PGC-1α expression is suppressed in diabetes (39,40). Because PGC-1α is parathyroid hormone responsive (41) in osteoblasts and its expression increases during osteoblast differentiation (42), we assessed its skeletal expression. Like Runx2, PGC-1α expression in wt but not *db* mice peaked at 12 weeks and then declined, and compared with wt, PGC-1α expression in *db* bones was significantly lower and showed significant decline with age (Fig. 3*A*).

Diabetes and obesity negatively influence muscular health by increasing atrogenes (43) that are involved in protein catabolism. Increasing PGC-1α expression and activity downregulates these atrogenes and prevents muscle atrophy under diverse stresses (44). Because some of

Downloaded from http://diabetesjournals.org/diabetes/article-pdf/64/7/2609/579698/db141611.pdf by guest on 14 May 2025

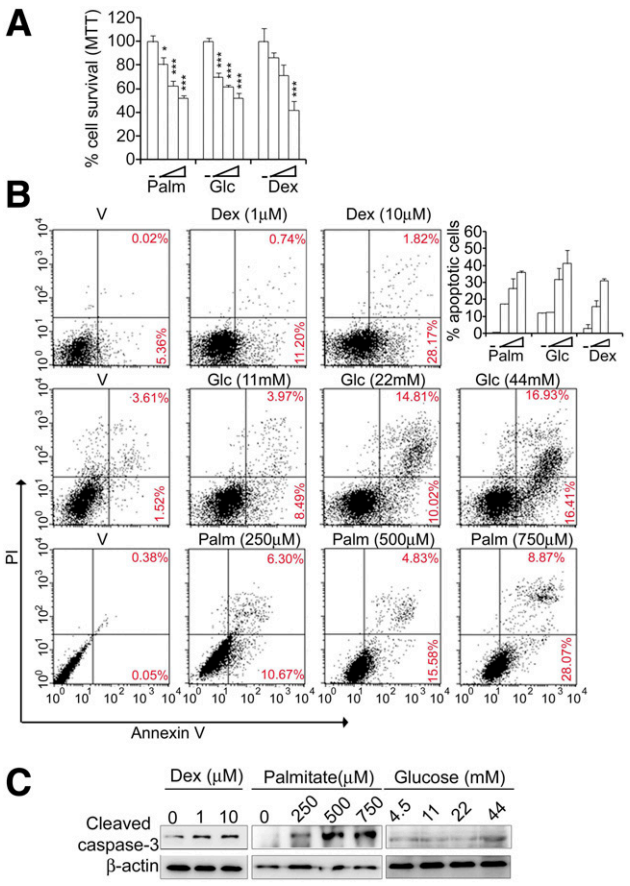

Figure 2—Glucose and free fatty acid (palmitate) are sufficient for inducing osteoblast apoptosis. *A*: Glucose and palmitate induce loss of osteoblast viability. MCOs were treated for 24 h as indicated, and cell viability was determined by an MTT assay and plotted as the percent of viable cells compared with vehicle-treated controls. Dex was used as positive control. The glucose and long-chain free fatty acid (palmitate) concentrations used here were based on available references (12,24,54,61). Data are mean ±SE of three independent experiments performed in triplicate. **P* < 0.05; ****P* < 0.001 compared with vehicle-treated control as determined by one-way ANOVA followed by Bonferroni posttest analysis. *B*: Glucose and palmitate induce osteoblast apoptosis in a concentration-dependent manner. MCOs were treated for 24 h as indicated, and apoptosis was analyzed by annexin V-FITC and PI staining followed by analysis in a FACSCalibur flow cytometer (Becton Dickinson). Representative dot plots are shown. The right panel shows quantification from two independent experiments. *C*: Palmitate but not glucose induces caspase-3 activation. MCOs were treated for 24 h as indicated, and cleaved caspase-3 levels were determined by immunoblotting. Data represent three independent experiments. Vehicle for Dex treatment was 0.1% DMSO. Vehicle for the glucose-treated group was medium containing 5.5 mmol/L glucose, and vehicle for the palmitate group was medium supplemented with 4% BSA. Glc, glucose; Palm, palmitate; V, vehicle.

these atrogenes are reported in bone and genetic ablations of the E3 ubiquitin ligase MuRF1 and lysosomal protease (cathepsin L) prevent unloading (45) and ovariectomy-induced bone loss (46), we assessed their skeletal expression. Compared with wt, *db* femur had significantly higher MuRF1, atrogin-1, and cathepsin L transcripts, and their levels in *db* but not wt mice increased significantly with age (Fig. 3*A*). Consistent with mRNA expression, PGC-1α protein level was drastically lower in *db* than wt mice of corresponding age-groups (Fig. 3*B*). Conversely, MuRF1 protein level was modestly higher in 8-week-old *db* mice than in wt mice but dramatically increased at 12 and 16 weeks (Fig. 3*B*).

Consistent with their ability to directly induce osteoblast apoptosis, palmitate or glucose alone robustly enhanced MuRF1 and atrogin-1 and decreased PGC-1α mRNA and protein in MCOs (Dex was used as positive control) (Fig. 3*C* and *D*).

Bones of Insulin-Resistant Mice Express Functional AdipoR1

We next asked whether modulating PGC-1α expression and activity could ameliorate diabetes-induced osteopenia. Adiponectin signaling through AdipoR1 in particular modulates PGC-1α (47,48); therefore, we first assessed its expression in wt and diabetic skeleton at various ages.

We recently reported that compared with B6.db, *db* mice at 12 weeks displayed severely depleted muscular AdipoR1 protein and impaired response to gAd (32). Of note, AdipoR1 was readily detectable in the wt, B6.db, and *db* bones, whereas consistent with our previous report (32), muscular AdipoR1 was markedly reduced in *db* but not B6.db mice (Fig. 4*A*). In agreement with differential AdipoR1 expression, acute gAd exposure caused AMPK phosphorylation in both muscle and bones of wt mice but only in bones of *db* mice (Fig. 4*B*).

To decipher intact AdipoR1 expression in bones from its depletion in *db* skeletal muscle, we assessed microRNA-221 (miR-221) and RNA binding protein polypyrimidine tract binding protein (PTB) levels because they negatively regulate AdipoR1 expression (49). miR-221 level in bone and muscle across all ages was significantly higher in both diabetic strains than wt, although compared with bone, differences in muscle was higher (two- to threefold in bone vs. three- to sixfold in muscle) (Fig. 4*C*). The PTB expression pattern, however, was different from miR-221. Although 8-week-old bones had similar PTB expression across groups, 12- and 16-week-old *db* bones displayed modest, but significantly higher PTB expression than both wt and B6.db (Fig. 4*C*). Skeletal muscle, however, showed a dramatically higher PTB expression in 12- and 16-week-old *db* mice (5- to 20-fold) than both wt and B6.db mice. Taken together, the PTB and miR-221 expression pattern appeared to correlate with the loss of AdipoR1 in skeletal muscle of *db* mice.

GTDF, an AdipoR1 Agonist, and Met Reverse Osteopenia in Diabetic Mice

We previously have shown that the osteoanabolic agent GTDF (23), acting as an AdipoR1 agonist, ameliorates diabetes in B6.db but not in *db* mice (32). Because AdipoR1 action in bone induces an osteogenic effect (50) and *db* bones were AdipoR1 intact (Fig. 4*A*), we reasoned that

Downloaded from http://diabetesjournals.org/diabetes/article-pdf/64/7/2609/579698/db141611.pdf by guest on 14 May 2025

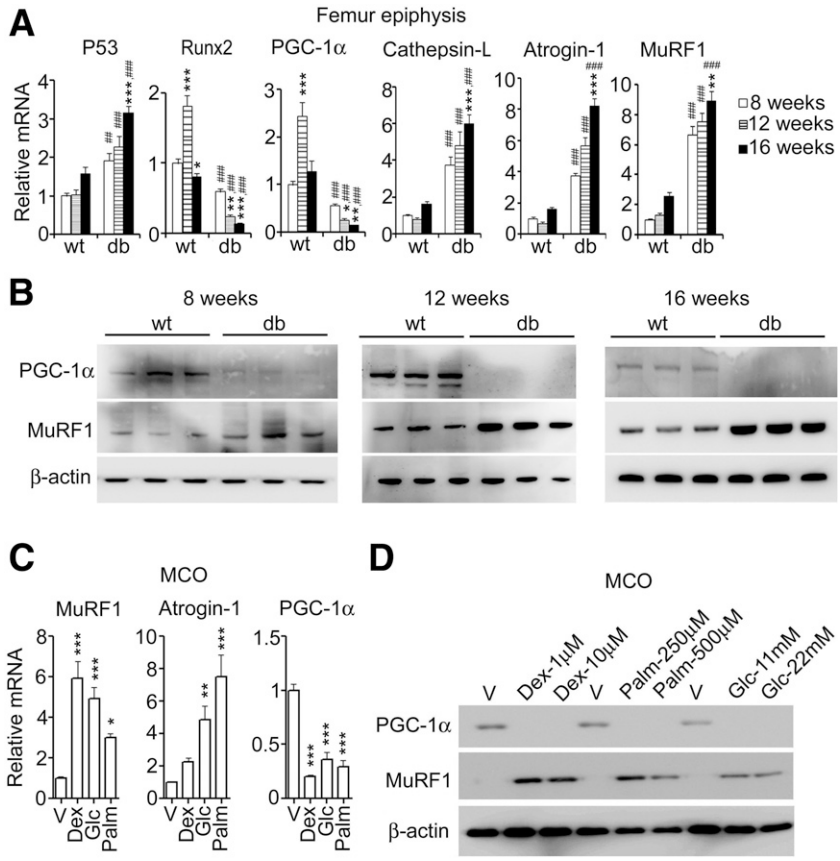

Figure 3—Diabetic bones exhibit enhanced skeletal muscle atrogenes and suppressed PGC-1α expression. *A*: qPCR-based gene expression analysis. Total RNA from femur epiphyses of indicated mice (n = 3/group) was isolated, reverse transcribed, and assessed for expression of indicated genes in triplicate. β-actin was used for normalization. Data are mean ± SE. *8-week vs. 12- or 16-week age-groups. #wt vs. *db*. $^{*}P < 0.05$; **,$^{\#\#}P < 0.01$; ***,$^{\#\#\#}P < 0.001$ as determined by two-way ANOVA followed by Bonferroni posttest analysis. *B*: Immunoblot evaluation of PGC-1α and MuRF1 protein levels in femur epiphyses. β-actin was used as loading control (n = 3). *C*: qPCR gene expression analyses in MCOs. MCOs were treated as indicated for 24 h, and mRNA expressions were analyzed. β-actin was used for normalization. Data are mean ± SE of three independent experiments performed in triplicate. $^{*}P < 0.05$; $^{**}P < 0.01$; $^{***}P < 0.001$ as determined by one-way ANOVA followed by Bonferroni posttest analysis. *D*: Evaluation of PGC-1α and MuRF1 expression by immunoblotting. β-actin was used as loading control. Data represent three independent experiments with similar results. Glc, glucose; Palm, palmitate; V, vehicle.

despite its inability to ameliorate diabetes, GTDF may still show an osteoanabolic effect in *db* mice.

Testing the effect of GTDF along with standard antidiabetic drugs necessitated a sufficient number of age- and sex-matched *db* mice that was not available in the present colony; thus, we procured fresh *db* mice with identical genetic background. This also allowed us to confirm that the skeletal phenotype observed in *db* mice (Fig. 1) were not due to breeding and maintenance-associated local factors. Trabecular and cortical parameters of both *db* mice were comparable (Supplementary Fig. 2*A* and *B*), and both displayed AdipoR1 expression in bone but not skeletal muscle (Supplementary Fig. 2*C*). These newly acquired *db* mice were then used for further studies.

We treated *db* mice with GTDF for 4 weeks at a dose (10 mg/kg) that failed to rescue diabetes in them (32), so any osteogenic outcome would not be a consequence of improved diabetic phenotype. We compared the skeletal effects of GTDF with clinically used antidiabetic drugs Met (AMPK/PGC-1α activator) and Pio (PPARγ agonist).

Assessment of metabolic parameters revealed that although final body weight significantly increased in Pio-treated mice as expected, GTDF or Met did not alter it (Supplementary Table 1). EchoMRI data showed that Pio but not GTDF or Met significantly increased fat mass, whereas none of the treatments altered lean mass or water content (Supplementary Table 1). Pio but not GTDF or Met significantly decreased fasting and nonfasting blood glucose levels, and Pio alone significantly reduced plasma triglyceride and VLDL levels (Supplementary Table 2).

In gross observation by μCT, deterioration of femoral and tibial trabecular architecture was readily observed in vehicle-treated *db* mice, whereas both GTDF and Met caused substantial improvement (Fig. 5*A*). Compared with vehicle-treated *db* mice, GTDF-treated *db* femur had significantly higher BV/TV, Tb.N, Tb.Th,

Downloaded from http://diabetesjournals.org/diabetes/article-pdf/64/7/2609/579698/db141611.pdf by guest on 14 May 2025

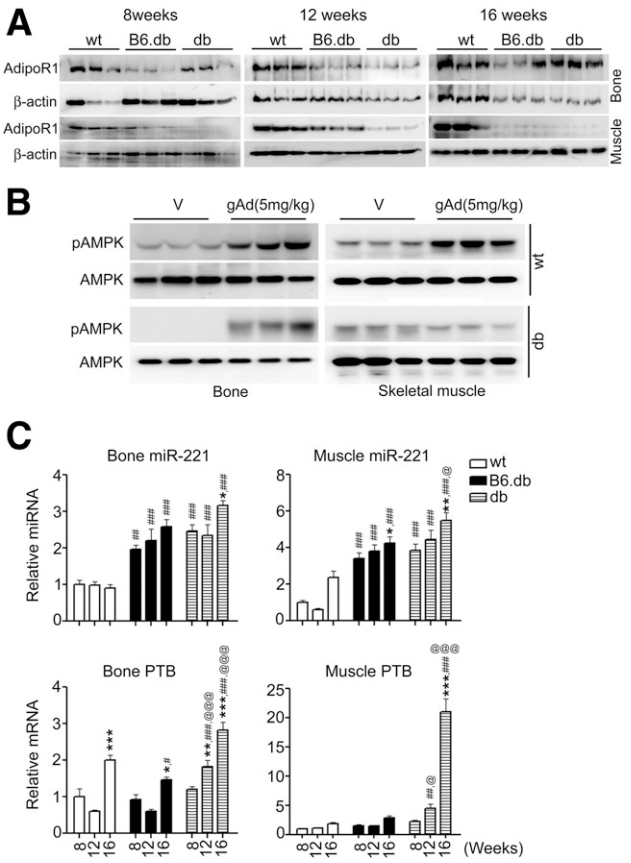

Figure 4—The *db* bones but not skeletal muscle express AdipoR1, bind to gAd, and induce AMPK phosphorylation. *A*: Evaluation of AdipoR1 protein level in wt or diabetic mice. Total protein was isolated from femur epiphysis or extensor digitorum longus muscles from wt, B6.db, or *db* mice, and AdipoR1 expression was determined by immunoblotting (n = 3). *B*: The *db* bones but not skeletal muscle displayed gAd sensitivity. The wt or *db* mice were intraperitoneally injected with vehicle (PBS) or gAd. Thirty minutes after injection, mice were killed, and total protein from extensor digitorum longus muscles and marrow-free femurs were used for determination of pAMPK and AMPK levels by immunoblotting (n = 3/group). *C*: Determination of age- and strain-dependent bone and skeletal muscle expression of PTB and miR-221. For miR-221, total miR from bone and gastrocnemius muscle was isolated using an miR isolation kit. miR-221 values were normalized with U6 expression and plotted. For PTB, total RNA isolated from the same tissues was used. Data are mean ± SEM of three independent experiments performed in triplicate. *8 week vs. 12- or 16-week age-groups; #wt vs. B6.db or *db*; @B6.db vs. *db*. *,#,@$P < 0.05$; **,##$P < 0.01$; ***,###,@@@$P < 0.001$ as determined by two-way ANOVA followed by Bonferroni posttest analysis. V, vehicle.

and Conn.D and lower Tb.Sp, and all the parameters were comparable to wt mice (Fig. 5*A*), suggesting complete trabecular restoration. Although BV/TV, Tb.N, and Tb.Th in the Met-treated group were restored to wt levels, these mice still had significantly lower Conn.D and higher Tb.Sp than wt mice (Fig. 5*A*), indicating a partial restoration. Pio modestly but significantly improved BV/TV, Tb.N, Tb.Th, and Conn.D in *db* femur but failed to reduce Tb.Sp, and except for Tb.Th and Tb.N, could not restore other parameters to wt levels (Fig. 5*A*). Tibial trabecular data show that except for Tb.Sp, all parameters in *db* mice were significantly lower than in wt mice (Fig. 5*A*). GTDF-treated *db* mice displayed significant improvement in all tibial parameters, and except for BV/TV and Tb.Sp, the rest were restored to wt levels (Fig. 5*A*), suggesting substantial tibial restoration. Met caused partial tibial restoration because only Tb.Th and Conn.D were comparable to wt (Fig. 5*A*). Pio was ineffective in restoring tibial cancellous bone because all parameters were lower than wt (Fig. 5*A*).

Biomechanical strength of femur diaphysis assessed by 3-point bending showed that *db* mice had significantly lower strength parameters than wt mice (data not shown) and that GTDF- and Met- but not Pio-treated *db* mice displayed significantly higher resistance to bending than vehicle-treated *db* mice, as evidenced from higher energy, failure load, and stiffness (Fig. 5*B*).

Furthermore, GTDF- and Met- but not Pio-treated *db* mice had higher periosteal cell numbers (Fig. 5*C* and Supplementary Fig. 3). Osteogenic effect of GTDF and Met was also evident from significantly higher Runx2 and OCN mRNAs in femur epiphysis of *db* mice treated with them, whereas Pio had no effect (Fig. 5*D*). Additionally, GTDF and Met but not Pio significantly lowered expression of adipogenic markers PPARγ and CCAAT-enhancer-binding protein α in *db* mice (Fig. 5*D*). In support of direct effects of GTDF and Met on osteoblasts, the cytotoxic and apoptosis-inducing effects of glucose and palmitate on osteoblasts were mitigated by GTDF and Met but not Pio (Fig. 5*E* and *F*).

AMPK is a key downstream mediator of AdipoR1 signaling, which phosphorylates and thereby activates PGC-1α (47). Osteoblasts in vehicle-treated *db* femur epiphysis had severely depleted pAMPK compared with wt (Fig. 6*A*). Consistent with the AdipoR1-intact status of diabetic bone, GTDF-treated *db* epiphysis had significantly higher pAMPK than vehicle-treated *db* (Fig. 6*A*). Met activates AMPK and, thereby, stimulates osteoblast differentiation (51,52), and consistent with this finding, Met-treated *db* mice displayed significantly higher pAMPK than vehicle controls (Fig. 6*A*). Pio-treated *db* also had modest but significantly higher pAMPK than vehicle-treated *db* (Fig. 6*A*). Similar to AMPK, PGC-1α expression in osteoblasts was severely lower in vehicle-treated *db* mice, and GTDF and Met but not Pio restored it (Fig. 6*A* and Supplementary Fig. 4). MuRF1 displays an inverse correlation with PGC-1α (Fig. 3) (44). In the current study, MuRF1 was also strongly expressed in vehicle-treated *db* osteoblasts, and in GTDF- and Met- but not Pio-treated *db* mice, its expression was significantly lowered (Fig. 6*A* and Supplementary Fig. 4). These results were confirmed by immunoblotting using whole marrow–free femur and tibia, where although PGC-1α was undetectable in vehicle- and Pio-treated *db* mice, it was strongly expressed in GTDF- or Met-treated *db* mice (Fig. 6*B*). Conversely, MuRF-1 level was high in vehicle- and Pio-treated *db* bones, whereas

Downloaded from http://diabetesjournals.org/diabetes/article-pdf/64/7/2609/579698/db141611.pdf by guest on 14 May 2025

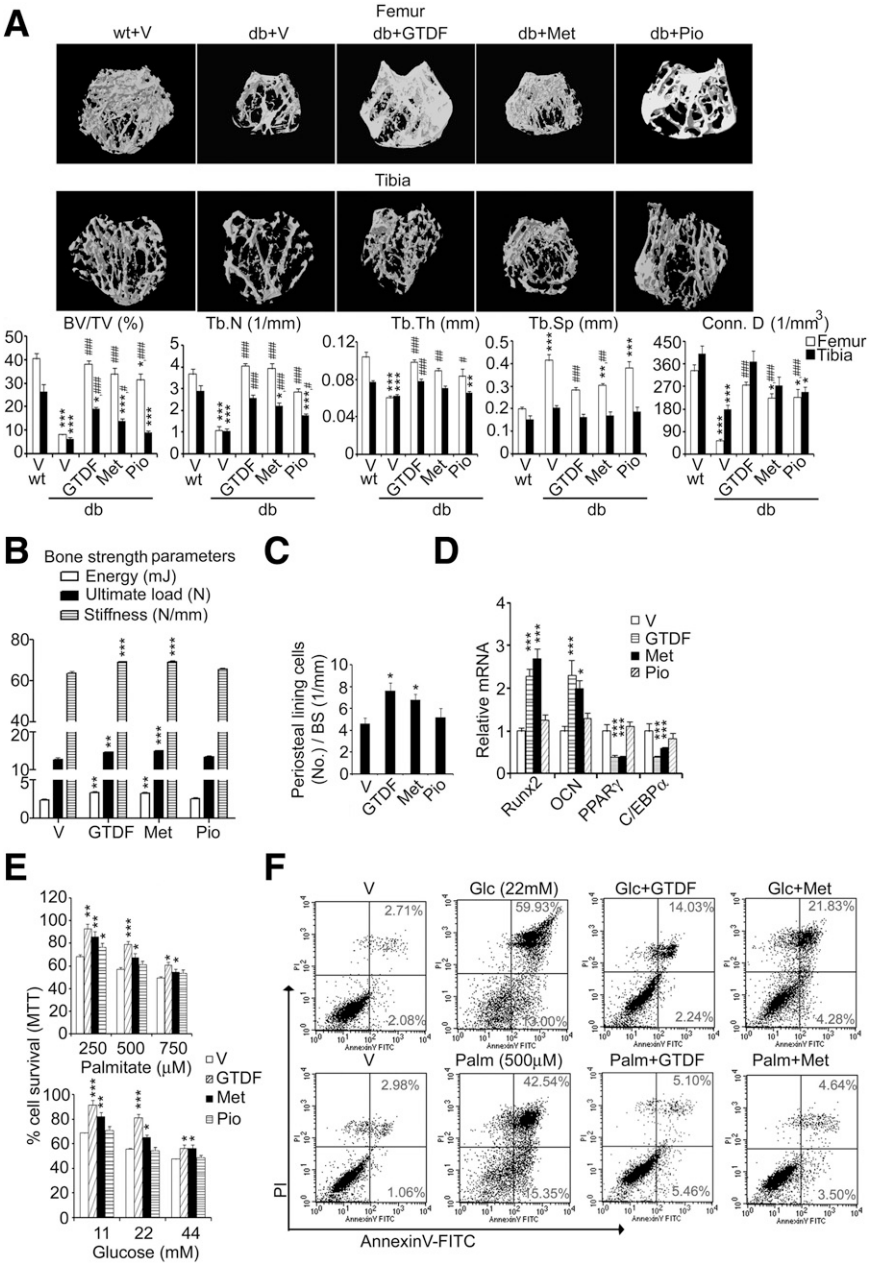

Figure 5—AdipoR1 agonist GTDF and AMPK/PGC-1α activator Met but not PPARγ agonist Pio improved bone phenotype in diabetic mice. Twelve-week-old *db* mice were treated with GTDF or Pio (10 mg/kg body weight) or Met (350 mg/kg body weight) for 4 weeks (comparison of skeletal parameters with *db* and AdipoR1 expression are shown in Supplementary Fig. 2*A*–*C*. Metabolic parameters and the plasma biochemistry are shown in Supplementary Tables 1 and 2). Data are mean ± SE. *wt vs. *db* (all treatments); #vehicle-treated *db* vs. other treatment groups. *A*: Evaluation of trabecular restoration by GTDF, Met, and Pio. Femur and tibia epiphyses from indicated animals (n = 10/group) were evaluated by μCT. Representative images are shown along with quantification data. *B*: Evaluation of bone strength. Bone strength parameters of the same animals were determined by 3-point bending test (n = 10/group). *C*: GTDF and Met but not Pio increased the number of trabecular lining cells. H-E–stained femur epiphysis sections (10 bones/group) were used for counting by two independent researchers blinded to the experimental design. Representative images are shown in Supplementary Fig. 3. *D*: GTDF and Met enhanced osteoblast formation markers and suppressed adipogenic marker expressions in femur epiphysis. Femur epiphysis from *db* mice (n = 3 performed in triplicate) treated as indicated were assessed for the expression of indicated mRNAs by qPCR. *E*: GTDF and Met but not Pio ameliorated palmitate- and glucose-induced loss of osteoblast viability. MCOs were pretreated with GTDF (0.1 μmol/L), Met (100 μmol/L), or Pio (1 μmol/L) for 24 h followed by treatment with indicated concentrations of glucose or palmitate for a further 24 h. Cell viability was then assessed by MTT assay. Data are mean ± SEM of three independent experiments performed in triplicate. *F*: GTDF and Met protect against palmitate and glucose-induced apoptosis. MCOs were pretreated with GTDF (0.1 μmol/L) or Met (100 μmol/L) for 24 h followed by 24-h incubation in medium containing the indicated concentration of glucose or palmitate. Apoptosis was assessed by annexin V-FITC and PI staining followed by flow cytometry. Representative dot plots from two independent experiments with similar results are shown. *Vehicle vs. treatment groups. *,#P < 0.05; **,##P < 0.01; ***,###P < 0.001 as determined by one-way ANOVA followed by Bonferroni posttest analysis. C/EBPα, CCAAT/enhancer–binding protein; Glc, glucose; Palm, palmitate; V, vehicle.

Downloaded from http://diabetesjournals.org/diabetes/article-pdf/64/7/2609/579698/db141611.pdf by guest on 14 May 2025

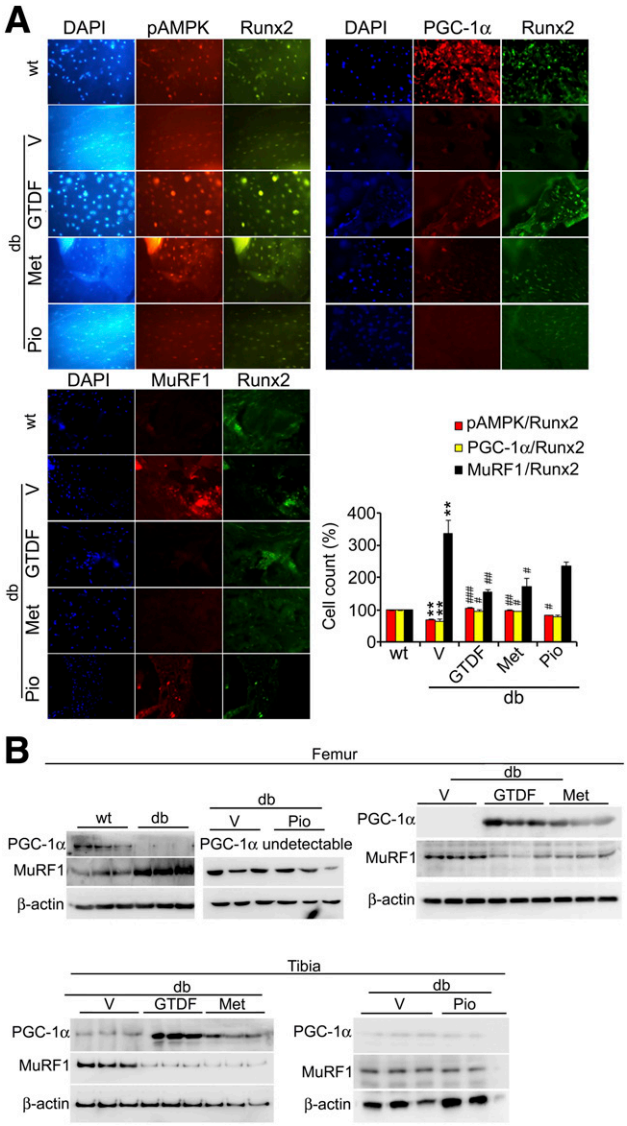

Figure 6—GTDF and Met but not Pio induce pAMPK and PGC-1α and suppress MuRF1 expression in *db* mice. *A*: Evaluation of osteoblast expressions of pAMPK, PGC-1α, and MuRF1. Femur epiphysis sections obtained from six mice per group were probed with indicated antibodies and visualized by fluorescent microscopy (Carl Zeiss Axio Imager.M2). Representative photomicrographs are shown (objective 20×, magnification 200×). Microscopic quantifications are percent cell count. *B*: PGC-1α and MuRF1 expression in femur or tibia epiphyses from mice treated as indicated (n = 3). *Comparison of *db* with wt mice. #Comparison between vehicle-treated *db* mice with GTDF-, Met-, or Pio-treated groups. #P < 0.05; **,##P < 0.01; ###P < 0.001 as determined by one-way ANOVA followed by Bonferroni posttest analysis. V, vehicle.

in GTDF- and Met-treated bones, it was drastically lower (Fig. 6*B*).

AdipoR1 and PGC-1α Mediate the Effects of GTDF in Osteoblasts

We next determined the roles of AdipoR1, AdipoR2, PGC-1α, and MuRF1 in osteoblasts by individually silencing them. Figure 7*A* shows confirmation of silencing of these proteins in osteoblasts.

MuRF1 depletion reduced both palmitate- and glucose-induced apoptosis in MCOs by >50% (Fig. 7*B*), suggesting the mediatory role of this atrogene in osteoblast apoptosis. We asked whether the protection conferred by GTDF against palmitate- and glucose-mediated MCO apoptosis (Fig. 5*G*) was AdipoR1 dependent. Indeed, siAdipoR1 but not siAdipoR2 or nonsilencing control siRNA (siC) abolished antiapoptotic effects of GTDF (Fig. 7*C* and Supplementary Fig. 5). siPGC-1α also abrogated the GTDF effect (Fig. 7*C*). As expected, the antiapoptotic effect of Met was attenuated by siPGC-1α but not siAdipoR1 (Fig. 7*C*).

Because both GTDF and Met restored trabecular and cortical parameters in *db* mice, which essentially indicated osteoanabolic actions of these compounds, we assessed GTDF- and Met-mediated osteoblast differentiation. In control MCOs (siC transfected), ALP activity was significantly stimulated by GTDF and Met (gAd and bone morphogenetic protein 2 [BMP-2] were used as positive controls for AdipoR1 and differentiation, respectively) (Fig. 7*D*). Silencing PGC-1α abolished the induction of ALP activity stimulated by all agents (Fig. 7*D*). Upon AdipoR1 silencing, the ALP stimulatory effect of gAd or GTDF but not BMP-2 was abolished (Fig. 7*D*). Silencing AdipoR2 failed to have an impact on the stimulatory effect of gAd or GTDF on ALP activity (Fig. 7*D*). These data suggest a specific role of AdipoR1 and PGC-1α in GTDF-mediated osteoblast differentiation. Of note, basal ALP activity in MCOs was also significantly depleted in the presence of siPGC-1α and siAdipoR1 but not siAdipoR2 (Fig. 7*D*), indicating that the autonomous activities of the two proteins might also be required for osteoblast differentiation.

DISCUSSION

Although there are numerous rodent models of type 2 diabetes, few have undergone thorough assessment of bone structure in relation to peak bone mass achievement and age-related bone loss. Among various mouse models that represent human obesity associated with type 2 diabetes, leptin receptor–deficient mice in a C57BLKS background represent severe phenotypes (53). In the current study, wt mice in C57BLKS background displayed peak bone mass achievement at both trabecular and cortical sites at 12 weeks, whereas *db* mice did not. Several reports have shown osteopenia in leptin receptor–deficient mice (6,13) with the exception of one (54), which showed high bone mass compared with wt littermates. The current data corroborate the finding of Williams et al. (36), showing trabecular osteopenia in ~11-week-old male *db* mice. In addition, *db* mice showed severe age-related bone loss. From these observations, it appears that *db* mice had an early termination of peak bone gain and/or early onset of age-related bone loss. Bone accrual critically depends on osteoblast number and function, and because *db* mice displayed robust apoptosis in osteoblasts at all ages, it appears that the lack

Downloaded from http://diabetesjournals.org/diabetes/article-pdf/64/7/2609/579698/db141611.pdf by guest on 14 May 2025

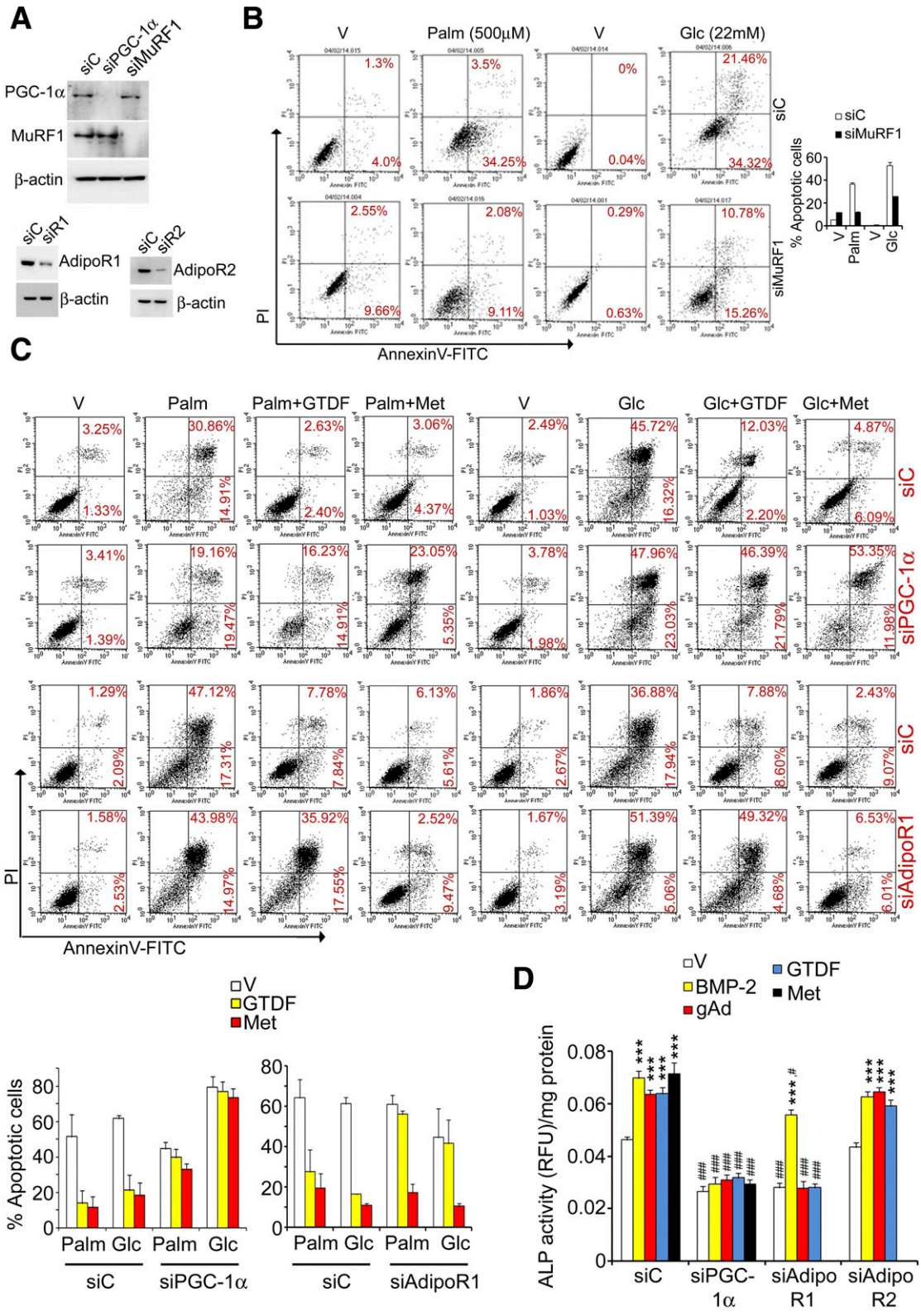

Figure 7—MuRF1 is necessary for palmitate- or glucose-induced osteoblast apoptosis, and AdipoR1 and PGC-1α are required for GTDF-induced protection against palmitate- and glucose-mediated osteoblast apoptosis. *A*: siRNA-mediated silencing of PGC-1α, MuRF1, AdipoR1, and AdipoR2. MCOs were transfected with 0.1 μmol/L of each siRNA, and expression of indicated proteins was assessed by immunoblotting. Data represent three independent experiments with similar results. *B*: MuRF1 depletion protects against glucose- and palmitate-induced osteoblast apoptosis. Forty-eight hours after transfection with indicated siRNAs, MCOs were incubated in medium containing indicated concentrations of Palm or Glc for a further 24 h. Apoptosis was then assessed by flow cytometry. One representative set of dot plots from two independent experiments is shown. The bar graph shows the quantification from two independent experiments (mean ± SE). *C*: GTDF protection against glucose- and palmitate-induced osteoblast apoptosis was compromised by AdipoR1 and

Downloaded from http://diabetesjournals.org/diabetes/article-pdf/64/7/2609/579698/db141611.pdf by guest on 14 May 2025

of viable osteoblasts and resultant deficiency in osteoblast function in the *db* bones was responsible for the failure in peak bone mass achievement and accelerated the development of age-related osteopenia. Bone formation is consistently lower in patients with type 2 diabetes compared with those without diabetes as evidenced by lower serum OCN (55), and as reported before (36), we observed that *db* mice also have markedly lower OCN levels at all ages than wt mice.

Glucose and palmitate induced mouse primary osteoblast apoptosis at pathologically relevant concentrations. The extent of cytotoxicity induced by palmitate and glucose was comparable to Dex, a potent inducer of osteopenia (33). It thus appears that the combined effect of glucotoxicity and lipotoxicity causes osteopenia equivalent in severity to that caused by Dex, and diabetic bones indeed shared common features of Dex-induced osteoporosis because bone was lost at both trabecular and cortical sites.

Tumor suppressor p53 is a negative regulator of osteoblast differentiation because it suppresses Runx2 expression, and hypermorphic p53 mutation in mice causes osteopenia (56). In *db* bones, p53 was increased and Runx2 suppressed, suggesting reduced osteoblast number and differentiation. Skeletal muscle atrogenes were also elevated in the *db* bones and showed an age-related increase, which could also negatively affect osteoblast survival and differentiation. In fact, silencing MuRF1 conferred robust protection against palmitate- and glucose-mediated MCO apoptosis. It is possible that other atrogenes (atrogin-1 and cathepsin L) also play key roles in osteopenia induced by various stresses because these factors were also induced in *db* bones and glucose- and palmitate-treated MCOs. Other reports support such a notion, as mice lacking these atrogenes are protected from osteopenia under diverse stresses (45,46). In contrast, the muscle anabolic factor PGC-1α exhibited an age-related decline in *db* mice. Therefore, it appears that like skeletal muscle, a reciprocal relationship between MuRF1 and PGC-1α exists in osteoblasts. Thus, loss of osteoblast population and function in *db* bones may occur due to suppression of PGC-1α and induction of atrogenes. The regulation and possible interaction of p53 and Runx2 with MuRF1 and PGC-1α would be an interesting future topic of investigation.

AdipoR1 increases insulin sensitivity and promotes cellular energy expenditure by activating AMPK and PGC-1α, and AdipoR1 activation represents an attractive therapeutic approach for the treatment of obesity and type 2 diabetes (48). Previously, we showed that *db* skeletal muscle is deficient in AdipoR1 expression (32). In contrast, we show here that diabetic bones are AdipoR1 intact. The explanation behind this appears to involve two negative AdipoR1 regulators, PTB and miR-221 (49), because both, especially PTB, were expressed at much higher levels in skeletal muscle than in bones of diabetic mice.

Adiponectin and its receptors are expressed in bone marrow stromal cells, which suggests their potential role in bone metabolism (57). C57BL6/J mice treated with adenoviral-derived adiponectin had increased trabecular bone mass and enhanced mineralization activity of osteoblasts (58). Mice harboring porcine AdipoR1 transgene had higher bone volume and trabecular numbers than age- and sex-matched controls (50). Cultures of bone marrow stromal cells from adiponectin knockout mice showed significantly less osteogenesis than cultures from adiponectin-intact mice (57). Together, these reports suggest that adiponectin may regulate bone formation in an autocrine/paracrine manner in addition to endocrine mode. Although AdipoR1 expression in *db* bones was comparable to wt, osteopenia in *db* mice could be attributed to their observed hypoadiponectinemia.

To investigate whether AdipoR1 in bone, and more specifically osteoblasts, of diabetic mice could be pharmacologically targeted to mitigate osteopenia through an osteoanabolic mechanism, we used GTDF. We have shown that GTDF improves diabetic phenotypes in B6.db mice with intact AdipoR1 in skeletal muscle and liver but not in *db* mice that lacked functional AdipoR1 in these tissues (32). Thus, *db* mice with skeletal (but not muscular) expression of functional AdipoR1 allowed us to selectively activate AdipoR1 in bone without correcting the diabetic phenotype. The most common clinically used drugs, Met and Pio, were used at their pharmacologically relevant doses for comparison of skeletal effects between the drugs.

Neither GTDF nor Met improved diabetic phenotypes in *db*, but Pio was modestly effective, although it

PGC-1α silencing. Forty-eight hours after transfection with indicated siRNAs, MCOs were incubated in medium containing glucose (22 mmol/L) or palmitate (500 μmol/L) supplemented with vehicle, GTDF (0.1 μmol/L), or Met (100 μmol/L) for a further 24 h. Apoptosis was then assessed by flow cytometry. One representative set of dot plots from two independent experiments is shown. The bar graph shows the quantification from two independent experiments. AdipoR2 silencing failed to influence GTDF or Met effects (Supplementary Fig. 5). *D*: GTDF- and gAd-mediated osteoblast differentiation depends on PGC-1α and AdipoR1 but not on AdipoR2. Forty-eight hours after transfection with indicated siRNAs, MCOs were incubated in differentiation medium supplemented with vehicle, GTDF (0.1 μmol/L), gAd (1 μg/mL), BMP-2 (0.1 μg/mL), or Met (100 μmol/L). Twenty-four hours after treatment, osteoblast differentiation was determined by fluorometric quantification of the differentiation marker ALP. Data are mean ± SE of three independent experiments performed in duplicate. *Vehicle vs. treatment groups, #siC vs. other siRNA-transfected groups. ***$P < 0.001$; #$P < 0.05$; ###$P < 0.001$ as determined by two-way ANOVA followed by Bonferroni posttest analysis. Glc, glucose; Palm, palmitate; RFU, relative fluorescence unit; siR1, siRNA against AdipoR1; siR2, siRNA against AdipoR2; V, vehicle.

Downloaded from http://diabetesjournals.org/diabetes/article-pdf/64/7/2609/579698/db141611.pdf by guest on 14 May 2025

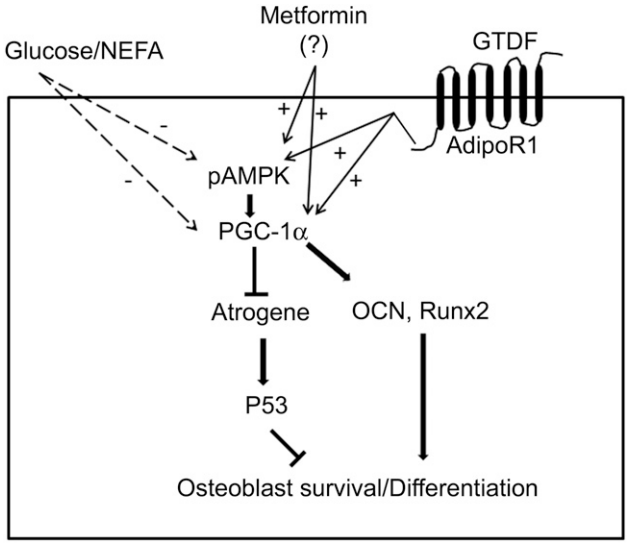

Figure 8—Schematic diagram summarizing the pathophysiological mechanisms of bone loss in *db* mice and a potential osteoanabolic role of AdipoR1. In osteoblasts, gluco- and lipotoxicity induce downregulation (−) of pAMPK and PGC-1α (a key regulator of cellular energy metabolism whose expression and activity are modulated by AdipoR1) and upregulation (+) of several skeletal muscle atrogenes (atrophy-related genes involved in protein catabolism), resulting in impaired survival and differentiation of these cells. Osteopenia in *db* mice is associated with reduced expression of osteogenic genes likely due to decreased PGC-1α and increased atrogenes. Atrogenes could in turn activate p53, leading to inhibition of osteoblast survival and function. Osteopenia in *db* mice could be reversed by GTDF (an AdipoR1 agonist) or Met (acting independent of AdipoR1 activation) but both converge to PGC-1α to promote osteogenic genes and suppress atrogenes that ultimately improve skeletal health by a likely osteoanabolic mechanism. →, stimulation; ⊣, inhibition.

failed to reduce NEFA levels but did reduce fasting and nonfasting serum glucose levels, which were still significantly higher than in wt. GTDF and Met improved trabecular microarchitecture and increased bone strength and bone lining cells. Pio was mostly ineffective because some improvement in femur epiphysis was seen, but tibia metaphysis, where bone is actually accrued less than in femur, showed no improvement. Additionally, strength parameters were not improved by Pio, and Pio did not increase periosteal cell number. The modest skeletal improvement by Pio could be due to modest mitigation of diabetic phenotypes because Pio failed to confer protection against gluco- and lipotoxicity on isolated osteoblasts. The skeletal improvement by GTDF and Met without altering diabetic phenotype as well as the protection imparted by them on isolated osteoblasts against glucose and palmitate assault clearly indicate that GTDF and Met had direct osteoblastic effects. The current data are also supported by previous reports where Met was shown to directly induce osteoblast differentiation (51,59) and protect against high-glucose–mediated inhibition of osteoblast growth (60).

Although both GTDF and Met restored bones of *db* mice by likely preserving osteoblasts against gluco- and lipotoxicity, the molecular mechanism of action of the two were different. Silencing AdipoR1 but not AdipoR2 abrogated the prosurvival and differentiation-promoting effects of GTDF, thus suggesting its AdipoR1-specific effect in osteoblasts as observed earlier in myocytes (32). Skeletal effects of Met, however, were blocked by silencing PGC-1α but not AdipoR1, suggesting that the osteoanabolic effect of the drug was mediated by PGC-1α and not AdipoR1, which was supported by Met failing to replace ^{125}I-gAd in a radioligand competition assay (data not shown). Salient findings of the current study are summarized in Fig. 8.

In conclusion, this study showed that diabetic mice in a BLKS background have poor achievement of peak bone mass and age-related development of severe osteopenia. Inducing and activating PGC-1α in osteoblasts by GTDF or Met completely reverse osteopenia in these mice without correcting diabetic phenotypes.

Acknowledgments. The authors acknowledge the sophisticated analytical instrument facility of the Central Drug Research Institute for help with confocal microscopy and flow cytometry. The authors also acknowledge technical support provided by Kavita Singh of the Sophisticated Analytical Instrument Facility, CSIR-Central Drug Research Institute for confocal microscopy.

Funding. M.P.K. and M.Y. were supported by the Indian Council of Medical Research. A.K.S. and A.G. were supported by fellowships from CSIR. S.Sh., H.K., J.S.M., and S.K. were supported by the University Grants Commission. S.Sa. and N.C. acknowledge funding from the CSIR Network project ASTHI (Anabolic Skeletal Targets in Health and Illness).

Duality of Interest. A.A.J. and M.R.J. are employees of Zydus Research Centre, the research and development arm of Cadila Healthcare Ltd. No other potential conflicts of interest relevant to this article were reported.

Author Contributions. M.P.K. contributed to the experimental design and performance, data analysis, and discussion. A.K.S. contributed to the experimental design, performance, and supervision; data analysis; and discussion. A.A.J., M.Y., S.Sh., H.K., A.G., J.S.M., M.C.T., G.K.N., and S.K. contributed to performing the experiments and to the data analysis and discussion. R.R., M.R.J., A.K.T., and R.M. contributed to supervising the experiments and to the data analysis and discussion. A.S. contributed to the data analysis and discussion. M.M.G. contributed to the experimental performance and supervision, data analysis, and discussion. J.R.G. contributed to the experimental design and supervision, data analysis, and discussion. S.Sa. contributed to the study concept, experimental design and supervision, data analysis, discussion, and writing of the manuscript. N.C. contributed to the experimental design and supervision, data analysis, discussion, and writing of the manuscript. N.C. is the guarantor of this work and, as such, had full access to all the data in the study and takes responsibility for the integrity of the data and the accuracy of the data analysis.

References

1. Janghorbani M, Van Dam RM, Willett WC, Hu FB. Systematic review of type 1 and type 2 diabetes mellitus and risk of fracture. Am J Epidemiol 2007;166:495–505

2. Bonds DE, Larson JC, Schwartz AV, et al. Risk of fracture in women with type 2 diabetes: the Women's Health Initiative Observational Study. J Clin Endocrinol Metab 2006;91:3404–3410

Downloaded from http://diabetesjournals.org/diabetes/article-pdf/64/7/2609/579698/db141611.pdf by guest on 14 May 2025

3. Kilpadi KL, Eldabaje R, Schmitz JE, et al. Type 2 diabetes is associated with vertebral fractures in a sample of clinic- and hospital-based Latinos. J Immigr Minor Health 2014;16:440–449
4. Viégas M, Costa C, Lopes A, Griz L, Medeiro MA, Bandeira F. Prevalence of osteoporosis and vertebral fractures in postmenopausal women with type 2 diabetes mellitus and their relationship with duration of the disease and chronic complications. J Diabetes Complications 2011;25:216–221
5. Schwartz AV, Vittinghoff E, Bauer DC, et al.; Study of Osteoporotic Fractures (SOF) Research Group; Osteoporotic Fractures in Men (MrOS) Research Group; Health, Aging, and Body Composition (Health ABC) Research Group. Association of BMD and FRAX score with risk of fracture in older adults with type 2 diabetes. JAMA 2011;305:2184–2192
6. Yamamoto M, Yamaguchi T, Yamauchi M, Kaji H, Sugimoto T. Diabetic patients have an increased risk of vertebral fractures independent of BMD or diabetic complications. J Bone Miner Res 2009;24:702–709
7. Hernandez RK, Do TP, Critchlow CW, Dent RE, Jick SS. Patient-related risk factors for fracture-healing complications in the United Kingdom General Practice Research Database. Acta Orthop 2012;83:653–660
8. Gooch HL, Hale JE, Fujioka H, Balian G, Hurwitz SR. Alterations of cartilage and collagen expression during fracture healing in experimental diabetes. Connect Tissue Res 2000;41:81–91
9. Topping RE, Bolander ME, Balian G. Type X collagen in fracture callus and the effects of experimental diabetes. Clin Orthop Relat Res 1994;308:220–228
10. Schwartz AV, Garnero P, Hillier TA, et al.; Health, Aging, and Body Composition Study. Pentosidine and increased fracture risk in older adults with type 2 diabetes. J Clin Endocrinol Metab 2009;94:2380–2386
11. Farr JN, Drake MT, Amin S, Melton LJ 3rd, McCready LK, Khosla S. In vivo assessment of bone quality in postmenopausal women with type 2 diabetes. J Bone Miner Res 2014;29:787–795
12. Patsch JM, Burghardt AJ, Yap SP, et al. Increased cortical porosity in type 2 diabetic postmenopausal women with fragility fractures. J Bone Miner Res 2013;28:313–324
13. Fajardo RJ, Karim L, Calley VI, Bouxsein ML. A review of rodent models of type 2 diabetic skeletal fragility. J Bone Miner Res 2014;29:1025–1040
14. Orland MJ, Permutt MA. Quantitative analysis of pancreatic proinsulin mRNA in genetically diabetic (*db/db*) mice. Diabetes 1987;36:341–347
15. Alberti G, Zimmet P, Shaw J, Bloomgarden Z, Kaufman F, Silink M; Consensus Workshop Group. Type 2 diabetes in the young: the evolving epidemic: the international diabetes federation consensus workshop. Diabetes Care 2004;27:1798–1811
16. Song SH, Hardisty CA. Early-onset Type 2 diabetes mellitus: an increasing phenomenon of elevated cardiovascular risk. Expert Rev Cardiovasc Ther 2008;6:315–322
17. Zeitler P, Hirst K, Pyle L, et al.; TODAY Study Group. A clinical trial to maintain glycemic control in youth with type 2 diabetes. N Engl J Med 2012;366:2247–2256
18. Pinhas-Hamiel O, Zeitler P. The global spread of type 2 diabetes mellitus in children and adolescents. J Pediatr 2005;146:693–700
19. Polonsky KS. Lilly Lecture 1994. The beta-cell in diabetes: from molecular genetics to clinical research. Diabetes 1995;44:705–717
20. Fajans SS, Bell GI, Polonsky KS. Molecular mechanisms and clinical pathophysiology of maturity-onset diabetes of the young. N Engl J Med 2001;345:971–980
21. Giuffrida FM, Reis AF. Genetic and clinical characteristics of maturity-onset diabetes of the young. Diabetes Obes Metab 2005;7:318–326
22. Pollock NK, Bernard PJ, Wenger K, et al. Lower bone mass in prepubertal overweight children with prediabetes. J Bone Miner Res 2010;25:2760–2769
23. Sharan K, Mishra JS, Swarnkar G, et al. A novel quercetin analogue from a medicinal plant promotes peak bone mass achievement and bone healing after injury and exerts an anabolic effect on osteoporotic bone: the role of aryl hydrocarbon receptor as a mediator of osteogenic action. J Bone Miner Res 2011;26:2096–2111
24. Reagan-Shaw S, Nihal M, Ahmad N. Dose translation from animal to human studies revisited. FASEB J 2008;22:659–661
25. Khan K, Singh A, Mittal M, et al. [6]-Gingerol induces bone loss in ovary intact adult mice and augments osteoclast function via the transient receptor potential vanilloid 1 channel. Mol Nutr Food Res 2012;56:1860–1873
26. Swarnkar G, Sharan K, Siddiqui JA, et al. A naturally occurring naringenin derivative exerts potent bone anabolic effects by mimicking oestrogen action on osteoblasts. Br J Pharmacol 2012;165:1526–1542
27. Bouxsein ML, Boyd SK, Christiansen BA, Guldberg RE, Jepsen KJ, Müller R. Guidelines for assessment of bone microstructure in rodents using micro-computed tomography. J Bone Miner Res 2010;25:1468–1486
28. Srivastava K, Khan K, Tyagi AM, et al. Greater skeletal gains in ovary intact rats at maturity are achieved by supplementing a standardized extract of *Butea monosperma* stem bark that confers better bone conserving effect following ovariectomy and concurrent treatment withdrawal. Evid Based Complement Alternat Med 2013;2013:519387
29. Gautam AK, Bhargavan B, Tyagi AM, et al. Differential effects of formononetin and cladrin on osteoblast function, peak bone mass achievement and bioavailability in rats. J Nutr Biochem 2011;22:318–327
30. Wong GL. Basal activities and hormone responsiveness of osteoclast-like and osteoblast-like bone cells are regulated by glucocorticoids. J Biol Chem 1979;254:6337–6340
31. Maniatopoulos C, Sodek J, Melcher AH. Bone formation in vitro by stromal cells obtained from bone marrow of young adult rats. Cell Tissue Res 1988;254:317–330
32. Singh AK, Joharapurkar AA, Khan MP, et al. Orally active osteoanabolic agent 6GTDF binds to adiponectin receptors, with a preference for AdipoR1, induces adiponectin-associated signaling and improves metabolic health in a rodent model of diabetes. Diabetes 2014;63:3530–3544
33. Khan MP, Mishra JS, Sharan K, et al. A novel flavonoid C-glucoside from *Ulmus wallichiana* preserves bone mineral density, microarchitecture and biomechanical properties in the presence of glucocorticoid by promoting osteoblast survival: a comparative study with human parathyroid hormone. Phytomedicine 2013;20:1256–1266
34. Weinstein RS, Manolagas SC. Apoptosis and osteoporosis. Am J Med 2000;108:153–164
35. Miller SC, de Saint-Georges L, Bowman BM, Jee WS. Bone lining cells: structure and function. Scanning Microsc 1989;3:953–960; discussion 960–961
36. Williams GA, Callon KE, Watson M, et al. Skeletal phenotype of the leptin receptor-deficient *db/db* mouse. J Bone Miner Res 2011;26:1698–1709
37. Harrity T, Farrelly D, Tieman A, et al. Muraglitazar, a novel dual (alpha/gamma) peroxisome proliferator-activated receptor activator, improves diabetes and other metabolic abnormalities and preserves beta-cell function in *db/db* mice. Diabetes 2006;55:240–248
38. Yamauchi T, Kamon J, Waki H, et al. The fat-derived hormone adiponectin reverses insulin resistance associated with both lipoatrophy and obesity. Nat Med 2001;7:941–946
39. Liang H, Ward WF. PGC-1alpha: a key regulator of energy metabolism. Adv Physiol Educ 2006;30:145–151
40. Coll T, Jové M, Rodríguez-Calvo R, et al. Palmitate-mediated downregulation of peroxisome proliferator-activated receptor-γ coactivator 1α in skeletal muscle cells involves MEK1/2 and nuclear factor-κB activation. Diabetes 2006;55:2779–2787
41. Nervina JM, Magyar CE, Pirih FQ, Tetradis S. PGC-1alpha is induced by parathyroid hormone and coactivates Nurr1-mediated promoter activity in osteoblasts. Bone 2006;39:1018–1025
42. Chen CT, Shih YR, Kuo TK, Lee OK, Wei YH. Coordinated changes of mitochondrial biogenesis and antioxidant enzymes during osteogenic differentiation of human mesenchymal stem cells. Stem Cells 2008;26:960–968
43. Akhmedov D, Berdeaux R. The effects of obesity on skeletal muscle regeneration. Front Physiol 2013;4:371

Downloaded from http://diabetesjournals.org/diabetes/article-pdf/64/7/2609/579698/db141611.pdf by guest on 14 May 2025

44. Sandri M, Lin J, Handschin C, et al. PGC-1alpha protects skeletal muscle from atrophy by suppressing FoxO3 action and atrophy-specific gene transcription. Proc Natl Acad Sci U S A 2006;103:16260–16265
45. Kondo H, Ezura Y, Nakamoto T, et al. MURF1 deficiency suppresses unloading-induced effects on osteoblasts and osteoclasts to lead to bone loss. J Cell Biochem 2011;112:3525–3530
46. Potts W, Bowyer J, Jones H, et al. Cathepsin L-deficient mice exhibit abnormal skin and bone development and show increased resistance to osteoporosis following ovariectomy. Int J Exp Pathol 2004;85:85–96
47. Iwabu M, Yamauchi T, Okada-Iwabu M, et al. Adiponectin and AdipoR1 regulate PGC-1alpha and mitochondria by Ca(2+) and AMPK/SIRT1. Nature 2010; 464:1313–1319
48. Yamauchi T, Kadowaki T. Physiological and pathophysiological roles of adiponectin and adiponectin receptors in the integrated regulation of metabolic and cardiovascular diseases. Int J Obes (Lond) 2008;32(Suppl. 7):S13–S18
49. Lustig Y, Barhod E, Ashwal-Fluss R, et al. RNA-binding protein PTB and microRNA-221 coregulate AdipoR1 translation and adiponectin signaling. Diabetes 2014;63:433–445
50. Lin YY, Chen CY, Chuang TY, et al. Adiponectin receptor 1 regulates bone formation and osteoblast differentiation by GSK-3β/β-catenin signaling in mice. Bone 2014;64:147–154
51. Molinuevo MS, Schurman L, McCarthy AD, et al. Effect of metformin on bone marrow progenitor cell differentiation: in vivo and in vitro studies. J Bone Miner Res 2010;25:211–221
52. Kanazawa I, Yamaguchi T, Yano S, Yamauchi M, Sugimoto T. Metformin enhances the differentiation and mineralization of osteoblastic MC3T3-E1 cells via AMP kinase activation as well as eNOS and BMP-2 expression. Biochem Biophys Res Commun 2008;375:414–419
53. Davis RC, Castellani LW, Hosseini M, et al. Early hepatic insulin resistance precedes the onset of diabetes in obese C57BLKS-*db/db* mice. Diabetes 2010; 59:1616–1625
54. Ducy P, Amling M, Takeda S, et al. Leptin inhibits bone formation through a hypothalamic relay: a central control of bone mass. Cell 2000;100: 197–207
55. Díaz-López A, Bulló M, Juanola-Falgarona M, et al. Reduced serum concentrations of carboxylated and undercarboxylated osteocalcin are associated with risk of developing type 2 diabetes mellitus in a high cardiovascular risk population: a nested case-control study. J Clin Endocrinol Metab 2013;98:4524–4531
56. Wang X, Kua HY, Hu Y, et al. p53 functions as a negative regulator of osteoblastogenesis, osteoblast-dependent osteoclastogenesis, and bone remodeling. J Cell Biol 2006;172:115–125
57. Shinoda Y, Yamaguchi M, Ogata N, et al. Regulation of bone formation by adiponectin through autocrine/paracrine and endocrine pathways. J Cell Biochem 2006;99:196–208
58. Oshima K, Nampei A, Matsuda M, et al. Adiponectin increases bone mass by suppressing osteoclast and activating osteoblast. Biochem Biophys Res Commun 2005;331:520–526
59. Jang WG, Kim EJ, Bae IH, et al. Metformin induces osteoblast differentiation via orphan nuclear receptor SHP-mediated transactivation of Runx2. Bone 2011; 48:885–893
60. Shao X, Cao X, Song G, Zhao Y, Shi B. Metformin rescues the MG63 osteoblasts against the effect of high glucose on proliferation. J Diabetes Res 2014; 2014:453940
61. Kim JE, Ahn MW, Baek SH, et al. AMPK activator, AICAR, inhibits palmitate-induced apoptosis in osteoblast. Bone 2008;43:394–404

Downloaded from http://diabetesjournals.org/diabetes/article-pdf/64/7/2609/579698/db141611.pdf by guest on 14 May 2025